6.829 Project Report: RF-Based Material Detection

Alejandro Perez
Massachusetts Institute of Technology

ABSTRACT

We present and evaluate a system that uses two directional antennas to estimate the location of different materials in a region of interest.

1. INTRODUCTION

Material detection is broad problem that has been studied for decades across numerous fields [1], [2], [3]. Several techniques have been developed and deployed for different applications. However, existing solutions rely on expensive and complicated hardware often ad-hoc to a specific well understood task. The development of a simpler solution has straightforward benefits like the reduction of cost. However, progress in this direction would also allow for new applications.

One could imagine using a system like this to detect the contents of unmarked boxes in an disorganized warehouse being searched for specific types of objects and contents. An expected measurement resulting from a specific material, say the metal of a concealed weapon, could allow for its detection by considering its difference to human body and clothing values. Similarly, collecting expected responses from say, humans and the structure of a building, could allow for many security and surveillance applications. Imaging specifically intended for the detection of a well understood type of material, e.g., computer hardware concealed in luggage, could become simpler and cheaper. Values for objects and materials could be collected and used for several purposes.

The goal of this project is to build and test a system for an application of this type.

2. RELATED WORK

The response specific materials have on signals has been studied for various applications. One example is the design of buildings intended for wireless communication. The NIST Construction Automation Program resulted on several reports on the attenuation of radio waves caused by different materials commonly found in buildings [4]. Similarly, the reflective coefficients of floor materials, e.g., wood, carpet, vinyl, have been measured in an effort to better understand their relationship to transmission loss [5]. Penetration loss and reflection have been also measured for different materials in New York City in an attempt to understand their effects on cellular communication at 28 GHz [6].

Some geophysical devices use radar pulses to image subsurfaces. Frequency-dependent attenuation coefficients can be estimated by analyzing data from Ground-penetrating Radar (GPR) for example. These values have been measured for materials like sand, clay and liquids [7]. Another measurement commonly estimated for these applications is the dielectric constant of different materials [8]. A GPR-based approach for the analysis of hot-mix-asphalt uses the information from reflected waves to calculate the thickness of a given material if the dielectric constant is known [9]. The publication also presents a method that uses the amplitude of the reflected signal to estimate the dielectric constant of a material in the case that the thickness is known.

Variants of the GPR device have been developed for pipe scanning. For example, the 'pipe penetrating radar' uses 1.6 and 2.3 GHz frequency antennas to detect holes in concrete pipes [10] and a similar solution uses of UWB antennas that transmit and receive electromagnetic pulses [11].

A useful measurement that has been widely studied for applied electromagnetic and stealth technologies is the Radar Cross-Section (RCS) [12]. This value depends largely on the material of an object (along with size and shape) and does not depend on emission strength or distance. Indeed, materials have been studied and evaluated directly in order to develop stealth-based buildings and vehicles not easy detected by radar [13], [14]. Additionally, several methods exist in the literature to measure the RCS values of different materials [15] and to estimate the RCS parameters of antennas [16].

An application recently presented uses RCS to detect pedestrians [17]. The publication describes an approach that considers radio wave reflections in the 76GHz band and presents their measurements of reflective intensity of different clothes. Another application is the detection of humans and furniture with a through-the-wall radar (TTWR) [18]. This TTWR application uses the finite difference time domain (FDTD) technique over the 1-5GHz frequency range to calculate RCS in order to more reliably distinguish humans from objects.

Other examples of material detection applications presented in the literature include the use of polarimetric radar techniques to detect large concealed weapons [19], an ultra-wideband short pulse radar imaging system that considers the effects of wall penetration and pulse fidelity for through-the-wall applications [20], and a proposed approach for cheaper imaging that relies on the analysis of backscatter as measured by radios found in household devices [21]. Finally, quantities like absorption coefficient, transmission coefficient, and index of refraction [22] characterize the behavior of waves in materials and are widely used for numerous electromagnetic applications [23].

In this project, we intend to leverage the ability to analyze and measure the effects different materials have on signals in order to relax the requirement of advanced and complicated hardware. We will explore the idea of moving the hardware with a robotic arm in hopes of getting more useful information from simple devices. We will also investigate if knowledge of shape and size of an area of interest is necessary. We have found several experiments in the literature where material properties have been measured with wireless signals (directly and indirectly). However, the use of this

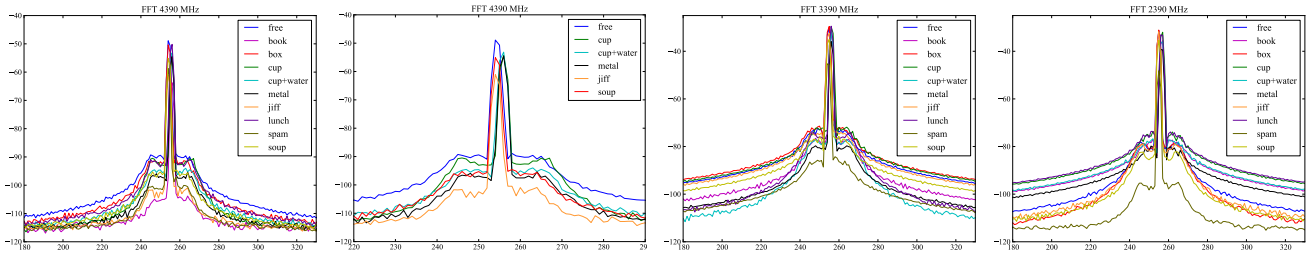

Figure 1: FFT plots showing the attenuation caused by several objects at 4390, 3390, and 2390 MHz respectively.

data to detect materials does not seem to be the goal for most of these applications.

3. APPROACH

In this section we present our proposed approach by describing its main components individually.

3.1 Material-Induced Loss

Propagating a signal through any medium results in reduction of power. However, signal loss can be due to multiple reasons, e.g., path loss, refraction, reflection, diffraction, absorption, scattering, alignment, etc. The proposed system estimates the loss caused by the transmission medium by maintaining several aspects of the resulting attenuation fixed and comparing the remaining difference. We consider the case where there are two directional antennas, one transmitting Tx, and one receiving Rx, separated by some distance d. We can use the Friis transmission equation [24] to represent the ratio in power between the antennas,

$$\frac{P^{\mathrm{Rx}}}{P^{\mathrm{Tx}}} = G^{\mathrm{Tx}} G^{\mathrm{Rx}} \left(\frac{\lambda}{4\pi d}\right)^2$$

where P^{Tx} and P^{Rx} are the power at Tx and Rx respectively, G^{Tx} and G^{Rx} are the antenna gains, d is the distance between the antennas, and λ is the wavelength at the transmitted frequency. Note that *free-space path loss*, i.e, the loss in signal strength in a line-of-sight path through free-space is $\mathrm{FSPL} = \left(\frac{4\pi d}{\lambda}\right)^2$ [25]. We can then calculate the received power when propagating through free-space by considering,

$$P^{\mathrm{Rx}}(d) = P^{\mathrm{Tx}} G^{\mathrm{Tx}} + G^{\mathrm{Rx}} - 20 \log 10 \left(\frac{4\pi d}{\lambda}\right)$$

Let $\bar{P}^{\mathrm{Rx}}(d)$ be the measured power when transmitting through free-space or a region of interest at distance d and $\tilde{P}^{\mathrm{Rx}}(d)$ be a second measurement taken s.t. $\left(\bar{\lambda} = \tilde{\lambda}\right) \wedge \left(\bar{G}^{\mathrm{Tx}} = \tilde{G}^{\mathrm{Tx}}\right) \wedge \left(\bar{G}^{\mathrm{Rx}} = \tilde{G}^{\mathrm{Rx}}\right) \wedge \left(\bar{P}^{\mathrm{Tx}} = \tilde{P}^{\mathrm{Tx}}\right)$. Then, we can estimate the *material-induced loss* by considering the difference,

$$\mathbb{L} = \bar{P}^{\mathrm{Rx}}(d) - \tilde{P}^{\mathrm{Rx}}(d).$$

The proposed system uses a narrow beam, therefore, $\mathbb{L}$ represents the loss caused by both absorption and scattering induced by the material.

3.2 Straight-line Scanning Trajectories

A correspondence between the measured loss and positions in the scanned space is needed in order to estimate the location of different materials in a region of interest. The proposed system uses two redundant manipulators to move two directional antennas along one axis. The resulting dual-arm trajectory maintains the antennas at a fixed distance and orientation as well as at equal positions in the remaining two axes while moving at a constant speed. The pose of each arm consists of seven joint angles, i.e., $j^{\mathrm{n}} = (\theta_1, \theta_2, \theta_3, \cdots, \theta_7) \in \mathbb{R}^7$, and a corresponding end-effector pose at this configuration $q^{\mathrm{n}} = (p, R)$ where $p^{\mathrm{n}} = (x, y, z)$ represents the translation, $R^{\mathrm{n}} = (q_0, q_1, q_2, q_3)$ is a Quaternion that represents rotation [26], and $f(.)$ is a mapping $q = f(j)$. Let d be the distance between the antennas during the scan, T be the desired time of the resulting scanning motion and $(q_i^{\mathrm{Rx}}, q_f^{\mathrm{Rx}}), (q_i^{\mathrm{Tx}}, q_f^{\mathrm{Tx}})$ be the initial and final poses of each end-effector. A straight-line scanning trajectory $j^{\mathrm{Rx}}, j^{\mathrm{Tx}} : [0, T] \in \mathbb{R}^7$ starts at $f(j^{\mathrm{Rx}}(0), j^{\mathrm{Tx}}(0)) = q_i^{\mathrm{Rx}}, q_i^{\mathrm{Tx}}$ and reaches $f(j^{\mathrm{Rx}}(T), j^{\mathrm{Tx}}(T)) = q_f^{\mathrm{Rx}}, q_f^{\mathrm{Tx}}$ with a sequence of configurations s.t. $\forall f(j^{\mathrm{Rx}}(t), j^{\mathrm{Tx}}(t)) \in [0, T]$

$$\left(p_x^{\mathrm{Rx}} = p_x^{\mathrm{Tx}}\right) \wedge \left(p_z^{\mathrm{Rx}} = p_z^{\mathrm{Tx}}\right)$$

$$p_y^{\mathrm{Rx}} = -p_y^{\mathrm{Tx}}$$

$$|p_y^{\mathrm{Rx}} - p_y^{\mathrm{Tx}}| = d$$

and,

$$\int_0^T \Delta R^{\mathrm{Rx}} + \Delta p_1^{\mathrm{Rx}} + \Delta p_2^{\mathrm{Rx}} = \int_0^T \Delta R^{\mathrm{Tx}} + \Delta p_1^{\mathrm{Tx}} + \Delta p_2^{\mathrm{Tx}} = 0$$

where p_1 and p_2 are the translation components corresponding to the fixed dimensions, i.e., x and y when scanning vertically and y and z when scanning horizontally.

3.3 Localized Attenuation

Real-time information regarding the received signal is recorded as the antennas move in the resulting straight-line scanning trajectory. More specifically, the discrete Fourier transforms (DFT) and all relevant data is continuously calculated by an FFT and corresponded to the location where the measurement took place. Let $\Sigma : [0, T]$ be a sequence of antenna poses with corresponding DFTs, i.e., $\sigma(t) = (q(t), \mathrm{DFT}(t))$, representing the measurements obtained while moving along a straight-line scanning trajectory with a total traversed distance of d_σ along the scanned axis. We divide the range into k segments $S = (s_i, \cdots, s_k)$ of distance $d_\Delta = \left(\frac{d_\sigma}{k}\right)$ s.t. $q_i \in s_i$ and $q_f \in s_k$ and assign all pose and DFT information in the sequence to its corresponding segment, i.e., $s_i := \{\sigma \in \Sigma : s_i^{p3} < q_{p3} < s_i^{p3} + d_\Delta\}$ where q_{p3} is the translation in the scanned dimension and s_i^{p3} is the location where the segment begins.

We calculate an estimate of the total power in each DFT by computing the sum squared amplitude [27],

$$P' = \sum_{i=0}^{N-1} A_i^2$$

where N is the number of frequency bins in the DFT. Each segment stores the mean of its associated DFTs as its power estimate. The sequence is then compared to a base sequence in order to estimate the attenuation at each segment.

For example, let $\bar{S}$ be a sequence of localized power estimates of size $k = 50$ obtained while scanning an empty container along the x-axis, i.e.,

$$\bar{S} = (P'_{\bar{s}_i}, \cdots, P'_{\bar{s}_k})$$

Let $\tilde{S}$ be a second sequence obtained when scanning the same container with a concealed object in an unknown location.

$$\tilde{S} = (P'_{\tilde{s}_i}, \cdots, P'_{\tilde{s}_k})$$

Finally, let $S_{\mathbb{L}}$ be the sequence with localized material-induced loss estimates resulting from taking the difference in received power measured during each sequence, i.e.,

$$S_{\mathbb{L}} = (\mathbb{L}_i = P'_{\bar{s}_i} - P'_{\tilde{s}_i}, \cdots, \mathbb{L}_k = P'_{\bar{s}_k} - P'_{\tilde{s}_k})$$

We can see that there is notable loss around segment s_{20}. Therefore, we can consider the possibility of a concealed object in the locations corresponding to segments $s_{19} - s_{25}$.

3.4 Material Identification

After attenuation is measured and localized, the material of the possible object can be estimated by considering the attenuation coefficients of several candidates. The total attenuation of an object of length l with an attenuation coefficient α can be calculated by considering

$$\xi = \alpha \cdot l \cdot f.$$

where f is the frequency [28]. Therefore, a list of possible materials can be created by using an upper bound and ruling out materials that are not able to cause the measured attenuation at a given transmission distance d (as l can not be larger than d if the object is located between the two antennas). More specifically, let ξ' be the measured attenuation at distance d, and let $\mathcal{A}$ be a list of attenuation coefficients of candidate materials (several lists are available in the literature and online [4], [29]). Then, the list of possible materials is

$$\dot{\mathcal{A}} = \{\alpha \in \mathcal{A} : \alpha \cdot d \cdot f \leq \xi'\}$$

The list can be further reduced by considering measurements taken at multiple distances and multiple frequencies, i.e., let Ω be list of measurement tuples $\omega = (\omega_d, \omega_f, \omega_\xi)$. The list of possible candidate materials can be represented as

$$\ddot{\mathcal{A}} = \{\omega_\alpha \in \Omega \times \mathcal{A} : \omega_\alpha \cdot \omega_d \cdot \omega_f \leq \omega_\xi\}$$

The coefficient of a material of interest can be estimated and used for future identification. The estimated attenuation coefficient for a measurment with an attenuation measurement ξ' taken with a transmission distance d and a wavelength λ of an object of length l can be represented as

$$\alpha' = \frac{\xi' - \left(\frac{4\pi d}{\lambda}\right)^2}{l \cdot f}$$

where $\text{FSPL} = \left(\frac{4\pi d}{\lambda}\right)^2$ is the free-space path loss [25].

Finally, if the attenuation coefficient is known, the length of the object can be estimated by considering

$$l' = \frac{\xi' - \left(\frac{4\pi d}{\lambda}\right)^2}{\alpha \cdot f}$$

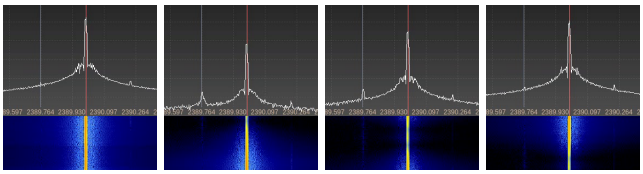

Figure 3: The real-time FFT readings shown as a metallic lunchbox with a concealed peanut butter container is scanned (see Figure 4). A decrease is visible in the spectrogram as well as in the FFT while the antennas move through the region with the object.

4. IMPLEMENTATION

We build and test a proof-of-concept scanning system that uses robotic arms to move two narrow beam directional antennas. The details are presented in this section.

4.1 Hardware

We use two USRP N210 radios with SBX 400-4400 MHz Rx/Tx daughterboards [30]. Both peripherals used WA5VJB 2.1-11GHz directional antennas [31]. The USRPs were connected to a single laptop using a Netgear Gigabit Ethernet switch. Each antenna is moved with a seven degree-of-freedom arm on a PR2 robot [32]. A Microsoft Kinect [33] infrared-based time-of-flight camera is used to record color and depth information.

An end-effector Cartesian controller is used to generate straight-line trajectories along a given axis. The controller takes the initial and final poses and linearly interpolates in Cartesian space between positions and orientations. Inverse kinematic solutions [34] are computed by using the Jacobian Pseudoinverse method [35]. The antennas are moved at a fixed orientation with a constant transmission distance of $d = .48$m. The horizontal scan moves the antennas for 0.37m forward and then returns to them to their initial position in a motion totaling in 15s. The vertical scan moves the antennas upward for 0.25m and then returns to them to their initial lower position in a motion totaling in 12s.

During the scanning motion, the transmitting antenna sends a constant signal and the receiving antenna takes continuous measurements. We test frequencies $f = 2390$MHz, 3390MHz, 4390MHz. All experiments were carried out in the G415 area in the Stata building.

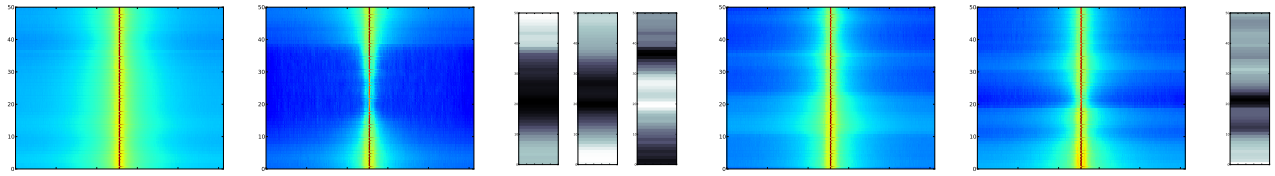

(a) (b) (c) (d)

Figure 2: (a) Spectrograms at each trajectory segment for a horizontal scan of free-space and a metallic box at 2390 MHz (see Figure 4). (b) Losses at each segment when scanning the metallic box and the metallic box with a concealed object along with the resulting difference. (c) Spectrograms at each trajectory segment for a horizontal scan of a plastic box and a plastic box with a concealed object (see Figure 7). (d) The resulting difference in loss at each segment for the measurements shown in (c).

4.2 Software

We use GQRX [36] and GNUradio [37] for real-time FFT computations and for I/Q recording and playback, the Robot Operating System (ROS) [38] to control the PR2 robot and to publish all relevant data, and ØMQ [39] to send the real-time FFT and I/Q readings to robot. We save images and point clouds [40] from the Kinect sensor on the robot along with the real-time pose of the arms.

We compute DFTs with a bin size of 512 at 60fps using GQRX. Each DFT is stored along with the correspoding pose (position and orientation) of each antenna. We divide each trajectory in $k = 50$ segments, which result in increment distances of $d_\Delta = \left(\frac{d_\sigma}{k}\right) = \left(\frac{0.37\text{m}}{50}\right) = 0.0074\text{m}$ and $d_\Delta = \left(\frac{d_\sigma}{k}\right) = \left(\frac{0.25\text{m}}{50}\right) = 0.005\text{m}$ for horizontal and vertical trajectories respectively.

5. EVALUATION

Material-Induced Loss: We measure the attenuation resulting from placing several objects between the two antennas. We record the DFT values estimated when transmitting at frequencies 2390, 3390, and 4390 MHz with a transmission distance of $d = .48\text{m}$.

Alignment Error: We test the ability of our system to maintain a fixed orientation, distance, and relative position between the two antennas while traversing scanning trajectories. We log position information for both end-effectors while performing several scanning trajectories and compute the difference in translation in the fixed axes.

5.1 Concealed Object Detection

We scan several containers with concealed objects and attempt to estimate their locations by considering regions with notable differences in transmission loss when compared to a baseline measurement. More specifically, we store a range-image of the scanned environment and compute the regions which show significant differences in loss. Because all measurements are coupled with their corresponding locations, we can render our estimate directly on the range-image and verify if the location is accurate. We test the following scenarios,

Metallic lunch box: A peanut butter container is placed inside a mettalic lunch box (see Figure 4, video).

Liquid detection: Five plastic cups are placed in a line with the second to last one containing water (see Figure 5, video).

Cardboard box: A peanut butter container and metallic plate are placed inside a cardboard box (see Figure 6).

Plastic box: A juice bottle and a soup can are placed inside a plastic lunch box (see Figure 7, video).

Textbook: A CD is placed between the pages of a closed textbook (see Figure 8, video).

Phone hidden in clothing: A phone is concealed in the front pocket of sweatshirt (see Figure 9, video).

6. RESULTS

Material-Induced Loss: Figure 1 shows the FFT plots for all objects at the different frequencies evaluated. The objects considered can be seen below.

These are shown in Figure 1 as `box`, `spam`, `lunch`, `metal`, `jiff`, `soup`, `book`, `cd`, `cup`, `juice`, `cup+water` and correspond to a cardboard box, a metallic box, a plastic box, a metallic plate, a peanut butter container, a soup can, a textbook, a CD, a plastic cup, a juice bottle, and a plastic cup with water respectively.

The plots in Figure 1 show that the attenuation caused by each object is distinct. Small differences, e.g., the difference in attenuation between an empty plastic cup and one with water, seemed to be easily registered. Indeed, we observed that the resulting attenuation caused by certain materials are similar to those measured in other publications [6], [4]. However, we also note that attenuation varied across frequencies. We only considered the frequencies in the 2-4.5 GHz range and took measurements at minimal transmission distance, yet the frequency seemed to play a substantial role in the resulting loss. It is clear that a system designed to robustly detect and localize objects in this frequency range should consider multiple frequencies simultaneously and to augment its analysis with other types of data. Another possible extension would be vary the transmission distance during the scan. Because the relationship between distance, wavelength, and object length is well understood, considering measurements from multiple transmission distances could improve the reliability of the system.

Alignment Error: We execute the horizontal and vertical trajectories described in the previous section several times and record the position information of both end-effectors.

These are published at approximately 60 Hz. For each position recorded, we compute and store the Euclidean distance between $\hat{p}^{\text{Rx}}$ and $\hat{p}^{\text{Tx}}$, i.e., $d_{\text{err}} = \|\hat{p}^{\text{Rx}} - \hat{p}^{\text{Tx}}\|$ where $\hat{p}^{\text{Rx}}$ and $\hat{p}^{\text{Tx}}$ are the positions of the receiving and transmitting antennas and $\hat{p}$ is the translation of x and z, i.e., $\hat{p} = (x, z)$, as y is fixed at the transmission distance d throughout the trajectory. A rendering of the observed error at each of the segments in the horizontal and vertical trajectories is below.

The highest distance between the antennas occurs at the end of the trajectory. This is possibly due to the vibration caused by the change in direction. Note that the robot moves the antennas in a straight-line and returns to the original position. One possible way to reduce this error is to slow down the transition between movements. We include the recorded minimum, maximum, and mean differences in position in the table below.

	Traj. Dist.	Step Size	Min. Diff.	Max. Diff.	Mean Diff.	Std. Dev.
x	0.37	0.0074	0.0026	0.014	0.0078	0.0024
z	0.25	0.005	0.0025	0.0064	0.0039	0.0011

Table 1: Recorded distances in position for horizontal (x) and vertical (z) trajectories.

The evaluated system uses Cartesian trajectories instead of directly specified joint-by-joint trajectories that could provide higher precision. This type of trajectories were used to allow for rapid computation and execution of straight-line scanning motions that are easily specified and require little engineering. This allows the system to be more general and adaptable to multiple scanning tasks but results in increased trajectory error.

We are currently exploring the possibility of using detailed antenna position and orientation information when calculating losses. This would improve the performance of the system and could also allow for more complicated scanning motions which could make it possible for a system to differentiate between losses that are caused by absorption from those caused by scattering and other effects.

More specifically, antenna gain can be related to *directivity* $D(\theta, \phi)$, i.e., $G = E_{\text{Rx}} D(\theta, \phi)$, and to gain in a particular direction, i.e, $G(\theta, \phi) = E_{\text{Rx}} D(\theta, \phi)$. Therefore, the geometric orientation of the antennas can be included directly in the Friis transmission equation [41]

$$\frac{P^{\text{Rx}}}{P^{\text{Tx}}} = E_{\text{Tx}} E_{\text{Rx}} \left(\frac{\lambda^2 D_{\text{Tx}}(\theta_{\text{Tx}}, \phi_{\text{Tx}}) D_{\text{Rx}}(\theta_{\text{Rx}}, \phi_{\text{Rx}})}{4\pi d} \right)^2$$

where E is the *antenna efficiency* [42] and direction is expressed as an elevation θ and azimuth ϕ.

Even though the current system logs all relevant directivity information and could easily be adapted to include scanning trajectories with multiple orientations, we leave this aspect of the analysis and corresponding experiments for future work.

6.1 Concealed Object Detection

We discuss the location estimates for the concealed objects described in the previous section.

Metallic lunch box: We take measurements during a horizontal scan at 2.39 GHz. Figure 4 shows the location of the concealed object along with two estimated locations and sizes corresponding to the box and the container inside (shown as the blue and green rectangles on the range-image respectively). The baseline measurement (empty metallic box) is shown in Figure 3.4 along with localized loss sequences for (i) difference of free-space and the empty box (ii) box with the concealed object and (iii) the difference of the empty box and the box with the concealed object. We observed that the size estimate corresponding to the metallic box was slightly larger than the object. Similarly, the estimate for the location of the concealed object begins a few segments after the actual location of the object and is smaller in size. Finally, we note that there is noticeable difference in loss at the beginning of the sequence. This effect seems to be only be present when the object is placed inside the metallic box. There are multiple possible causes for this difference such as reflections and alignment error. More measurements would be required in order to truly isolate these types of effects.

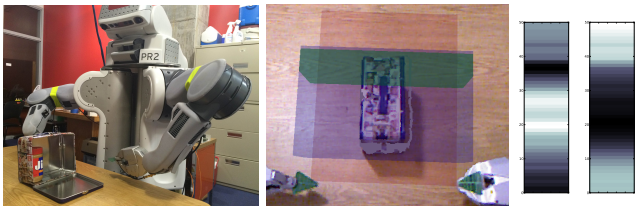

Figure 4: Horizontal scan of a metallic box with a concealed peanut butter container at 2.39 GHz. The estimated location and size of the box and object are displayed in the range-image as the blue and green rectangles respectively. The loss sequences used for the estimates are shown besides the range-image.

Liquid detection: We attempt to detect the presence of liquid inside several plastic cups. We scan the cups horizontally at 4.39 GHz. The resulting estimate is shown in Figure 5. This estimate was computed by considering the difference in loss between a free-space scan and the scan of the plastic containers. The difference in loss occurs at the correct location, allowing the estimate to detect the cup containing water. We note a difference at the beginning of the sequence similar to that seen in the loss sequence for the metallic box. Reflections and initial vibration are possible causes for this measurement.

Cardboard box: We scan a cardboard box with two concealed objects, a metallic plate and a peanut butter container, at 4.39 GHz. Figure 6 shows the estimated location and size of the peanut butter container on the range-image taken with the box and on the range-image taken when the box was removed. We used a free-space scan as the baseline as we were not able to obtain significant power loss information when scanning the empty box. The resulting location estimate correctly detects the location of the container within the box. However, we notice a slight shift in the x-axis which also seems to be present in other tests. We then scan for a second object, a metallic plate, which was placed

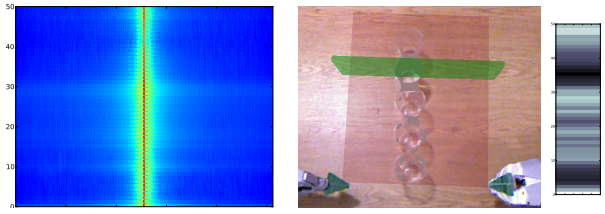

Figure 5: Horizontal scan of several plastic cups (one with water) at 4.39 GHz. The spectrograms measured at each location are shown on the left. A estimated size and location of the cup containing water is shown as a green rectangle in the range-image. The loss sequence used for the estimate is shown besides the range-image. This sequence is the result of the difference in loss between a free-space scan and the scan of the cups.

towards the center of the box (not pictured). The loss sequence computed when comparing to a free-space baseline is below.

The estimated size and location of the metallic plate was accurate. We note that this scan was particularly clear as the attenuation caused by cardboard and metal at 4.39 GHz is significantly different.

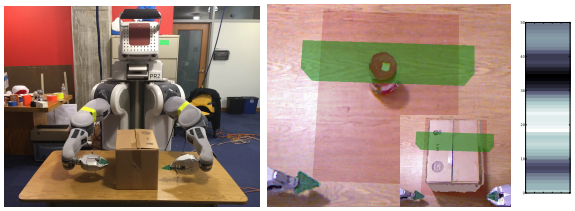

Figure 6: Horizontal scan of a cardboard box with a concealed object. The estimated size and location of the object is shown on the range-image taken with the box as well as on the range-image taken when the box was removed. The loss sequence used for the estimate is shown on the right.

Plastic box: We scan a plastic lunch box at 3.39 GHz and attempt to detect two concealed objects, a juice bottle and a soup can. We noticed that we were unable to get significant measurements when scanning the empty box. Therefore, free-space scans were used as the baseline. Figure 7 shows the estimated location and size of the juice bottle (green) and the soup can (blue). The location of the juice bottle was fairly accurate. However, changing the concealed object seemed to greatly affect the signal response.

We noticed that the loss sequences computed for the soup can were not consistent with the rest of the results obtained during this round of tests. We use the collection of segments corresponding to the region with the highest difference for the estimate (approximately located at $s_{15} - s_{30}$). This results in a roughly accurate estimate of the object (shown next to the range-image in 7). Yet, we observe several substantial differences in power elsewhere in the sequence. We are unable to characterize this measured behavior but suspect it might be caused by scattering and reflections induced by the materials and shapes in this particular scenario.

We include several loss sequences for completeness. These correspond to the differences in loss between scans of the box containing the soup can and the free-space scans at frequencies 2.39 GHz, 3.39 GHz, and 4.39 GHz respectively. They are shown below.

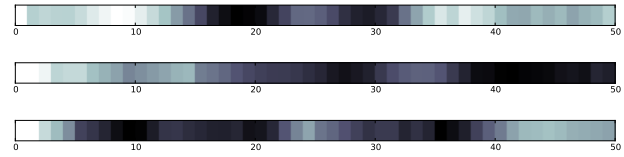

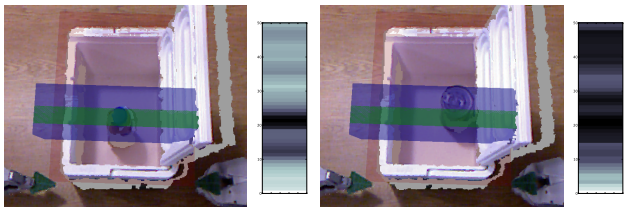

Figure 7: Estimated locations of a juice bottle and soup can within a plastic lunch box displayed on the range-image as green and blue respectively. Measurements were taken at 3.39GHz.

Textbook: We perform a horizontal scan at 4.39 GHz in order to attempt to localize a CD placed inside a closed textbook. Figure 8 shows the arrangement of the objects (the CD is slightly visible in the image on the left). We use a scan of the textbook without the disc as a baseline. The resulting loss sequence has a region with notable decrease (segments $s_5 - s_{19}$) which includes the highest difference in the sequence at its center (segments $s_{12} - s_{13}$). We show the considered loss sequences below. These correspond to the scan taken with the textbook, the scan of the textbook with the CD, and finally the difference in loss between these two.

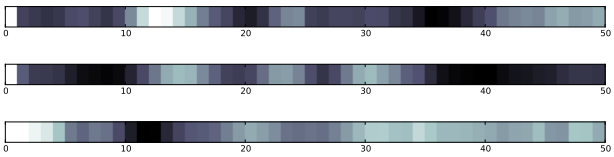

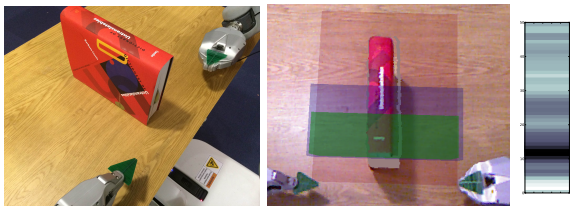

Figure 8: A CD is hidden inside a textbook. The estimated location of the disc is shown on the range-image as a green rectangle. The loss sequence used for the estimate is shown on the right. The scan was performed at 4.39 GHz.

Phone hidden in clothing: In order to test the feasibility of using a system of this type to detect an object in an unknown region (i.e., one for which a baseline scan is not available) we attempt to localize a phone concealed in the front pocket of sweatshirt. A vertical scan is performed at 2.39 GHz while a human subject stands between the antennas. We use a free-space scan as our baseline. The resulting sequence is shown in Figure 9. The region with the most significant difference corresponds to the location of the concealed phone.

We are able to observe a second region above the estimated location. The cause of this second difference in loss is not clear given the available information. One possible way to increase the reliability of the estimates is to consider the attenuation coefficients of the human body [29] and to use size information (from a range-image or by using the transmission distance as an upper bound) to estimate the expected power loss. We leave a more detailed evaluation of the use of this system for this type of applications for future work.

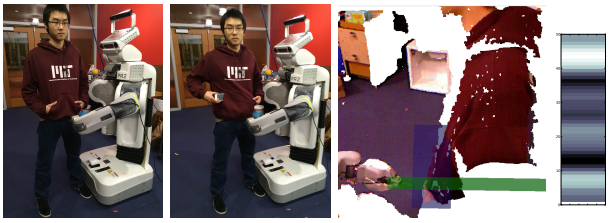

Figure 9: A vertical scan is performed at 2.39 GHz. The estimated location of the concealed object is shown as a green rectangle on the range-image. The loss sequence is shown on the right.

7. CONCLUSION

We presented and evaluated a proof-of-concept implementation of our proposed system. Our limited results are somewhat encouraging as detection and coarse localization was possible with minimal measurements and basic analysis. We expect that it is possible to relax the hardware requirements further by expanding the analysis to consider multiple aspects in more detail. We suggest several potential extensions to the approach in the report.

8. REFERENCES

[1] Laurence A Manning. The theory of the radio detection of meteors. *Journal of Applied Physics*, 19(8):689–699, 1948.

[2] Lyle A French, John J Wild, and Donald Neal. Detection of cerebral tumors by ultrasonic pulses. pilot studies on postmortem material. *Cancer*, 3(4):705–708, 1950.

[3] VI Matveev, VP Kozlov, VM Budov, and Yu V Seskutov. Use of uhf radio waves to check the internal structure of refractories. *Glass and Ceramics*, 27(7):397–401, 1970.

[4] W. C. Stone, National Institute of Standards, and Technology (U.S.). *NIST Construction Automation Program Report No. 3: Electromagnetic Signal Attenuation in Construction Materials*. U.S. Dept. of Commerce, Technology Administration, National Institute of Standards and Technology Gaithersburg, Md, 1997.

[5] J. Ahmadi-Shokouh, S. Noghanian, E. Hossain, M. Ostadrahimi, and J. Dietrich. Reflection coefficient measurement for house flooring materials at 57-64 ghz. In *Global Telecommunications Conference, 2009. GLOBECOM 2009. IEEE*, pages 1–6, Nov 2009.

[6] Hang Zhao, Rimma Mayzus, Shu Sun, Mathew Samimi, Jocelyn K. Schulz, Yaniv Azar, Kevin Wang, George N. Wong, Felix Gutierrez Jr., and Theodore S. Rappaport. 28 ghz millimeter wave cellular communication measurements for reflection and penetration loss in and around buildings in new york city. In *ICC*, pages 5163–5167. IEEE, 2013.

[7] John H. Bradford. Frequency-dependent attenuation analysis of ground-penetrating radar data. *Geophysics, Vol. 72, No. 3.*

[8] H.S. Nalwa. *Handbook of Low and High Dielectric Constant Materials and Their Applications: Phenomena, properties, and applications*. Handbook of Low and High Dielectric Constant Materials and Their Applications. Academic Press, 1999.

[9] Amara Loulizi, Imad L Al-Qadi, and Samer Lahouar. Optimization of ground-penetrating radar data to predict layer thicknesses in flexible pavements. *Journal of transportation engineering*, 129(1):93–99, 2003.

[10] C. Ekes and B. Neducza. Pipe condition assessments using pipe penetrating radar. In *Ground Penetrating Radar (GPR), 2012 14th International Conference on*, pages 840–843, June 2012.

[11] A. Jaganathan, E. Allouche, and N. Simicevic. Pipeline scanning: Novel technology for detection of voids and internal defects in non-conductive buried pipes. In *Proceedings of the No-Dig Down Under*, Oct 2006.

[12] M. I. Skolnik. *Introduction to Radar Systems 2nd Edition*. McGraw Hill Book Co., New York, 2 edition, 1980.

[13] Paul Saville. Review of radar absorbing materials. Technical report, DTIC Document, 2005.

[14] K.J. Vinoy, K.J. Vinoy, and R.M. Jha. *Radar absorbing materials: from theory to design and characterization*. Number v. 1. Kluwer Academic Publishers, 1996.

[15] R.B. Dybdal. Radar cross section measurements. *Proceedings of the IEEE*, 75(4):498–516, April 1987.

[16] S. Shrestha, M. D. Balachandran, M. Agarwal, Li-He Zou, and K. Varahramyan. A Method to Measure Radar Cross Section Parameters of Antennas. *Antennas and Propagation, IEEE Transactions on*, 56(11):3494–3500, 2008.

[17] N. Yamada, Y. Tanaka, and K. Nishikawa. Radar cross section for pedestrian in 76GHz band. In *Microwave, European Conference*, 2005.

[18] Travis D. Bufler, Ram M. Narayanan, and Traian Dogaru. Radar signatures of indoor clutter for through-the-wall radar applications. *Proc. SPIE*, 9077:90770E–90770E–11, 2014.

[19] T. Dogaru, C. Le, and U.S. Army Research Laboratory. *Through the Wall Small Weapon*

Detection Based on Polarimetric Radar Techniques. ARL-TR. Army Research Laboratory, 2009.

[20] Yunqiang Yang and Aly E. Fathy. See-through-wall imaging using ultra-wideband short-pulse radar system. *Proc. IEEE Antennas Propagation Soc. Int'l Symp. Digest*, pages 96–337, 2005.

[21] Dinesh Bharadia, Kiran Raj Joshi, and Sachin Katti. Full duplex backscatter. In *Proceedings of the Twelfth ACM Workshop on Hot Topics in Networks*, HotNets-XII, pages 4:1–4:7, New York, NY, USA, 2013. ACM.

[22] L.C. Shen and J.A. Kong. *Applied electromagnetism*. Brooks/Cole Engineering Division, 1983.

[23] Vladmir Bulovic, Rajeev Ram, Steven Leeb, Jeffrey Lang, and Yu Gu. Reflection and transmission of em waves. MIT Open Courseware, 2011.

[24] H. T. Friis. Friis transmission equation. In *Proceedings of the IEEE vol. 34*, page 234, 1946.

[25] IEEE standard definitions of terms for antennas. Technical report, 1993.

[26] William R. Hamilton. On Quaternions, or on a New System of Imaginaries in Algebra. *Philosophical Magazine*, 25(3):489–495, 1844.

[27] Masako Izumi and Shin ichi Izumi. Integrability theorem for fourier series and parseval equation. *Journal of Mathematical Analysis and Applications*, 18(2):252 – 261, 1967.

[28] J.R. Wait. The attenuation vs frequency characteristics of vlf radio waves. *Proceedings of the IRE*, 45(6):768–771, June 1957.

[29] Absorption Coefficients α of Building Materials and Finishes. http://www.sengpielaudio.com/calculator-RT60Coeff.htm.

[30] USRP N210. http://ettus.com, Ettus Inc.

[31] WA5VJB antenna. http://www.wa5vjb.com/, Kent Electronics.

[32] PR2: Robot for Research and Innovation. https://www.willowgarage.com/pages/pr2/overview, Willow Garage.

[33] Microsoft Kinect. http://www.microsoft.com/en-us/kinectforwindows/.

[34] R.P. Paul. *Robot Manipulators: Mathematics, Programming, and Control : the Computer Control of Robot Manipulators*. MIT Press series in artificial intelligence. MIT Press, 1981.

[35] Samuel R. Buss. Introduction to inverse kinematics with jacobian transpose, pseudoinverse and damped least squares methods. In *IEEE Journal of Robotics and Automation*, pages 681–685, 2004.

[36] GQRX SDR, A software defined radio powered by GNU-Radio and Qt. http://http://gqrx.dk.

[37] GNURadio, The Free and Open Software Radio Ecosystem. http://gnuradio.org/redmine/projects/gnuradio/wiki.

[38] ROS: The Robot Operating System. http://www.ros.org/.

[39] ZeroMQ. http://zeromq.org/.

[40] PCL - The Point Cloud Library. http://pointclouds.org/.

[41] C.A. Balanis. *Antenna Theory: Analysis and Design*. Wiley, 2012.

[42] Ieee standard definitions of terms for antennas. *IEEE Std 145-1993*, pages 1–32, July 1993.